NASA TECHNICAL NOTE

NASA TN D-3522

NASA TN D-3522

EXPERIMENTS TO DETERMINE THE STRENGTH OF FILAMENT-WOUND CYLINDERS LOADED IN AXIAL COMPRESSION

by Michael F. Card

Langley Research Center
Langley Station, Hampton, Va.

NATIONAL AERONAUTICS AND SPACE ADMINISTRATION • WASHINGTON, D. C. • AUGUST 1966

DISCLAIMER NOTICE

THIS DOCUMENT IS BEST QUALITY AVAILABLE. THE COPY FURNISHED TO DTIC CONTAINED A SIGNIFICANT NUMBER OF PAGES WHICH DO NOT REPRODUCE LEGIBLY.

NASA TN D-3522

EXPERIMENTS TO DETERMINE THE STRENGTH OF FILAMENT-WOUND CYLINDERS LOADED IN AXIAL COMPRESSION

By Michael F. Card

Langley Research Center
Langley Station, Hampton, Va.

NATIONAL AERONAUTICS AND SPACE ADMINISTRATION

For sale by the Clearinghouse for Federal Scientific and Technical Information
Springfield, Virginia 22151 – Price $2.00

EXPERIMENTS TO DETERMINE THE STRENGTH OF FILAMENT-WOUND CYLINDERS LOADED IN AXIAL COMPRESSION

By Michael F. Card
Langley Research Center

SUMMARY

Results of compression tests conducted on 51 multilayered glass-epoxy cylinders are presented. Tests were conducted at both room temperature and elevated temperatures on cylinders having various helical wrap angles, matrix materials, and diameters. Experimental results indicate that, in some of the cylinders, failures were induced by buckling whereas, in others, failures were induced by thermal degradation and/or nonlinearity in the stiffness of the matrix material in the cylinder wall. The data obtained from the unheated cylinders are compared with buckling predictions based on linear anisotropic shell theory and with material strength predictions based on anisotropic yield criteria. The comparison indicated that agreement obtained between buckling tests and theoretical predictions was comparable to that obtained in previous experience with metal cylinders and that strength predictions were overly conservative. The results suggest that the compressive strength of a filament-wound cylinder can be limited by its material strength and that more refined material strength analyses are needed for multilayered fibrous composites loaded in axial compression.

INTRODUCTION

Filament-wound structures are currently being evaluated for a variety of structural applications. Although originally developed to resist high internal pressures, filament-wound cylindrical shells have been proposed for structures in which axial compression or external pressure are the principal loadings. (See refs. 1 and 2.) At present, little experimental information on the strength of filament-wound cylinders under such loadings is available. For compressive loading, references 3 to 6 contain a major portion of the available data.

The purpose of the present paper is to report the results of an experimental investigation of the compressive strength of 51 glass-epoxy, multilayered filament-wound cylinders. The cylinder walls consisted of several alternating helically and circumferentially wrapped layers. Variables in the test program included cylinder diameter, epoxy,

helical wrap angle, and wall temperature. A few preliminary results from the test program are presented in reference 7. A selected group of the test cylinders was employed in an experimental investigation of elastic moduli of filament-wound cylinders reported in reference 8.

In certain of the test specimens, failures were a consequence of buckling of the cylinder wall whereas in others failure was influenced by material degradation due to temperature and/or nonlinearity of the stiffnesses in the epoxy matrix. Estimates of the relative importance of each of the two types of failure modes are made by comparing the experimental data obtained from unheated cylinders with theoretical predictions. The data are compared with approximate material strength predictions by using existing anisotropic yield criteria (refs. 9 and 10) and with buckling calculations based on anisotropic shell theory (ref. 11). As a consequence of asymmetry of the layers of the cylinder wall about the shell middle surface, coupling between membrane and bending behavior was present in the test specimens. The magnitude of coupling effects is assessed by a comparison between buckling solutions in which coupling is considered with solutions in which coupling is neglected.

SYMBOLS

The units used for the physical quantities in this report are given both in U.S. Customary Units and in the International System of Units (SI). A table of conversion factors is given in appendix A. The relationship between these two systems of units can be found in reference 12.

A_{ij} defined in equation (C4)

a_{ij} defined in equation (B3)

C contiguity factor (see ref. 14)

C_{ij} extensional constants of cylinder wall (see eq. (8.6), p. 34, ref. 11)

C_x, C_y, C_{xy} approximate extensional and shearing stiffnesses of cylinder wall (see eqs. (C7))

D_{ij} bending constants of cylinder wall (see eq. (8.8), p. 35, ref. 11)

D_x, D_y, D_{xy} approximate bending constants of cylinder wall (see eqs. (C7))

E	Young's modulus
E_L, E_T	Young's modulus of unidirectional layer in direction parallel and perpendicular to fibers, respectively
E_x, E_y	approximate Young's moduli of cylinder wall (see eqs. (B9) of ref. 8)
E_x', E_y'	Young's moduli for anisotropic layer of multilayered composite (see eqs. (B1) and (B2))
$\overline{E}_x, \overline{E}_y$	equivalent Young's moduli for helically wrapped layer of cylinder wall
G_{LT}	shearing modulus of unidirectional layer
G_{xy}	approximate shear modulus of cylinder wall $\overline{G}_{xy}\overline{t}_h + G_{LT}\left(1 - \overline{t}_h\right)$
G_{xy}'	shear modulus of anisotropic layer of multilayered composite (see eqs. (B1) and (B2))
$\overline{G}_{xy}$	equivalent shear modulus for helically wrapped layer of cylinder wall
K_{ij}	coupling constants of cylinder wall (see eq. (8.7), p. 35, ref. 11)
k	constant associated with anisotropic yield criteria (see eq. (1))
l	length of cylinder
M_x	additional axial moment per unit length during buckling
m	number of half waves in cylinder buckle pattern in longitudinal direction
m_1, m_2	elastic constants of anisotropic layer defined by eqs. (B1) and (B2)
N_x	additional axial force per unit length during buckling
$\overline{N}_x, \overline{N}_y, \overline{N}_{xy}$	applied axial, circumferential, and shear forces per unit length, respectively
n	number of full waves in cylinder buckle pattern in circumferential direction

P_{max}	compressive strength where P is axial load
p	total number of layers in multilayered composite
r	radius of cylinder
S	allowable shearing strength of unidirectional layer associated with directions parallel and perpendicular to fiber
T	temperature
t	thickness of cylinder wall
$\bar{t}$	fraction of thickness of cylinder wall occupied by a layer
$\bar{t}_h$	fraction of thickness of cylinder wall occupied by helically wrapped layers
u,v,w	buckling displacements in x-, y-, and z-directions, respectively
v_f	glass volume fraction
X,Y	allowable strength of unidirectional layer in directions parallel and perpendicular to fibers, respectively
x,y	orthogonal curvilinear coordinates (see fig. 1)
α	helical wrap angle (see fig. 1)
γ	shearing strain
ϵ	normal strain
μ_L,μ_T	Poisson's ratios of a unidirectional layer of the cylinder wall associated with normal stresses parallel and perpendicular to the fibers, respectively
μ	Poisson's ratio
μ_x,μ_y	Poisson's ratios of cylinder wall associated with normal stresses in x- and y-directions, respectively

$\tilde{\mu}_x, \tilde{\mu}_y$ Poisson's ratios of cylinder wall associated with bending stresses in x- and y-directions, respectively

μ'_x, μ'_y Poisson's ratios of anisotropic layer of multilayered composite associated with normal stresses in x- and y-directions, respectively

$\overline{\mu}_x, \overline{\mu}_y$ equivalent Poisson's ratios of helically wrapped layer of cylinder wall associated with normal stresses in x- and y-directions, respectively

ρ density

σ normal stress

τ shear stress

Superscript:

(i) ith layer of p-layer composite

Subscripts:

f fiber

i ith layer of p-layer composite

L,T directions parallel and perpendicular to fibers, respectively

m matrix

x,y longitudinal and circumferential directions, respectively

av average

max maximum

A subscript preceded by a comma denotes partial differentiation with respect to the subscript.

EXPERIMENTAL INVESTIGATION

Test Specimens

The geometry of the test specimens is indicated in figures 1 and 2. The cylinder shown in figure 1 is constructed by wrapping filaments in alternating helical and

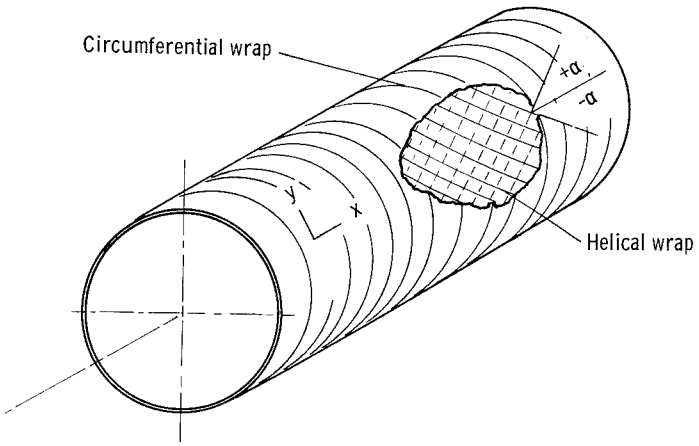

Figure 1.- Overall geometry of filament-wound cylinder.

circumferential layers. The helically wrapped layers are composed of two half layers, with filaments oriented at the angles $+\alpha$ or $-\alpha$ measured from the cylinder axis. The ends of the cylinders are reinforced to prevent end failures. The wall geometry of the test specimens is indicated in figure 2 which is a photomicrograph of a typical wall section of one of the test specimens. The cylinder wall is composed of six alternating helically and circumferentially wrapped layers consisting of glass filaments embedded in an epoxy matrix. The filaments are about 0.0003 inch (8 μm) in diameter so that there are roughly 30 000 filament sections appearing in the segment shown.

The test specimens consisted of 51 glass-epoxy cylinders. Variables in the specimens were the helical wrap angle α, the cylinder matrix material, and the cylinder radius r. The dimensions and material details of the cylinders are presented in tables I, II, and III. For convenience, the cylinders having a diameter of 2.6 inches (6.6 cm) are referred to as tubes, whereas those with a diameter of 15 inches (38 cm) are referred to as cylinders. As mentioned previously, certain of the test specimens were employed in the experiments reported in reference 8. The tubes employed in reference 8 correspond to tubes 1 to 8 of table II of the present paper and the cylinders 1 to 11 of table III.

The values of wall thickness t shown in tables II and III are the average of several measurements taken at random. The scatter in individual measurements was about ±3 percent of the value listed and was attributed to the irregular outer surface of the test

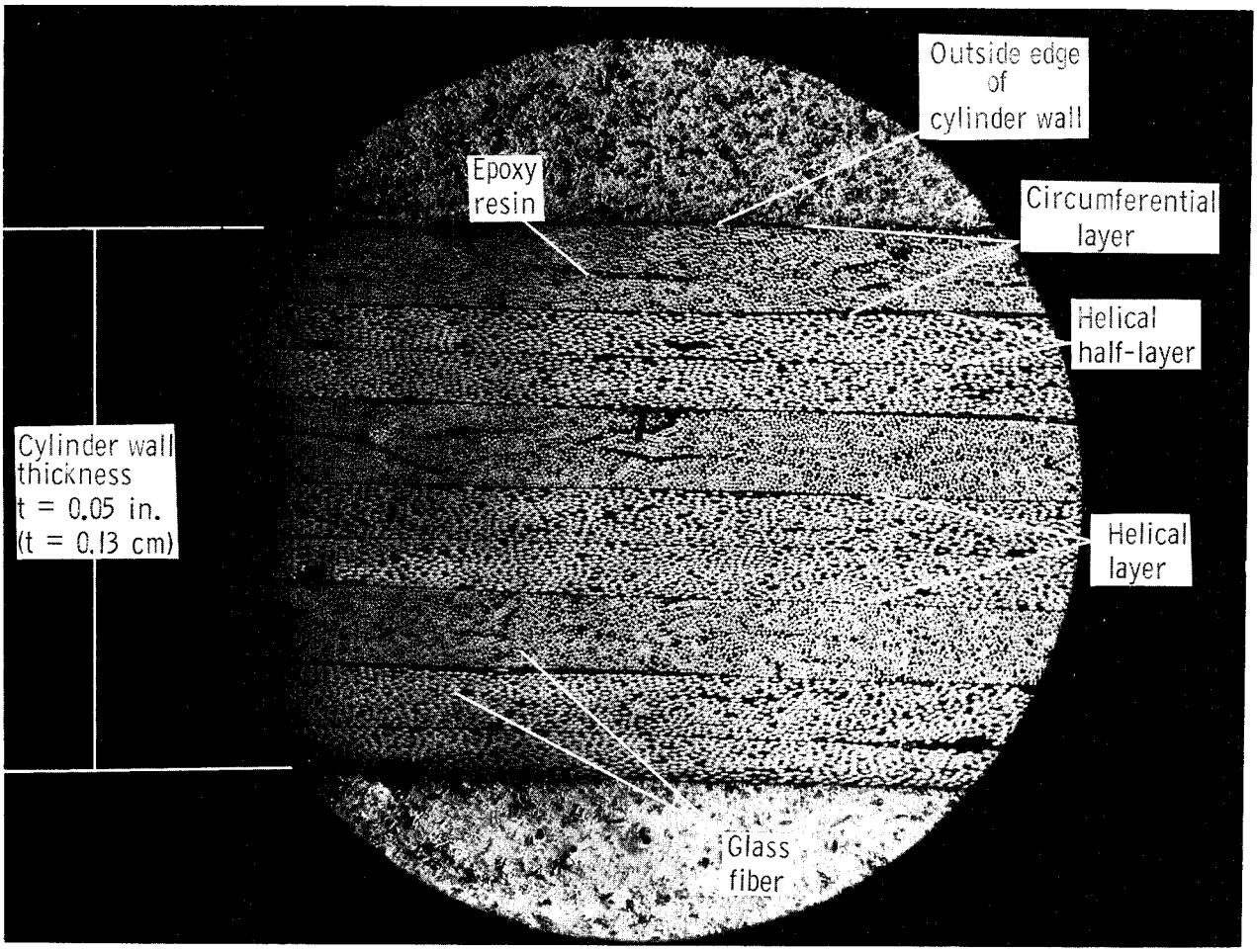

Figure 2.- Photomicrograph of wall of filament-wound cylinder. L-65-199.1

specimens. The values of the volume fraction of glass v_f listed in the tables were obtained from elevated-temperature exposures of three or four coupons cut from the wall of each specimen. The coupons were subjected to a temperature of 1100° F (866° K) for a period of 3 hours. On the basis of some preliminary tests in which weight loss was measured continuously, the temperature and time were determined to be sufficient to permit virtually all the resin in the coupon to decompose. The remaining glass was weighed and the equivalent glass volume fraction v_f was calculated by using the values of density quoted in table I. The scatter in calculated values of v_f was ±3 percent of the value given in tables II and III.

All the test specimens were loaded in compression between the platens of a testing machine. The ends of the specimens were ground flat and parallel prior to testing, and the specimens were carefully alined to insure uniform bearing between the ends of the

specimens and the platens of the testing machine. Tests on the tubes were conducted at room temperature whereas tests on cylinders were conducted at both room and elevated temperatures.

Tube Tests

Before the compression tests, all the tubes were exposed to small torsion loads to determine their shearing stiffness. (See ref. 8.) For the present tests, the ends of all the tubes were reinforced to prevent end failures by the addition of a layer of glass cloth about 1 inch (2.5 cm) wide and of thickness equal to twice that of the tube wall. The use of reinforcement was prompted by preliminary tests in which tubes 3 and 6 failed in bearing. The damaged ends of these tubes were subsequently removed and the tubes were retested with reinforced ends.

The tubes were loaded to failure at a slow rate (3.6 kips/min (0.27 kN/s) without cycling. The compressive strengths P_{max} of the tubes are given in table II. Measurements of axial strain were made during the tests and are presented in reference 8. The stress-strain curves obtained were characterized by varying degrees of nonlinearity above a stress level of about 6 ksi (41 MN/m^2). During loading, soft tinkling sounds could be heard over the upper third of the loading range. Failure of the tubes was accompanied by a cracking noise and the appearance of a series of splits around the circumference of the tube. Figure 3 is a photograph of all the tubes after failure.

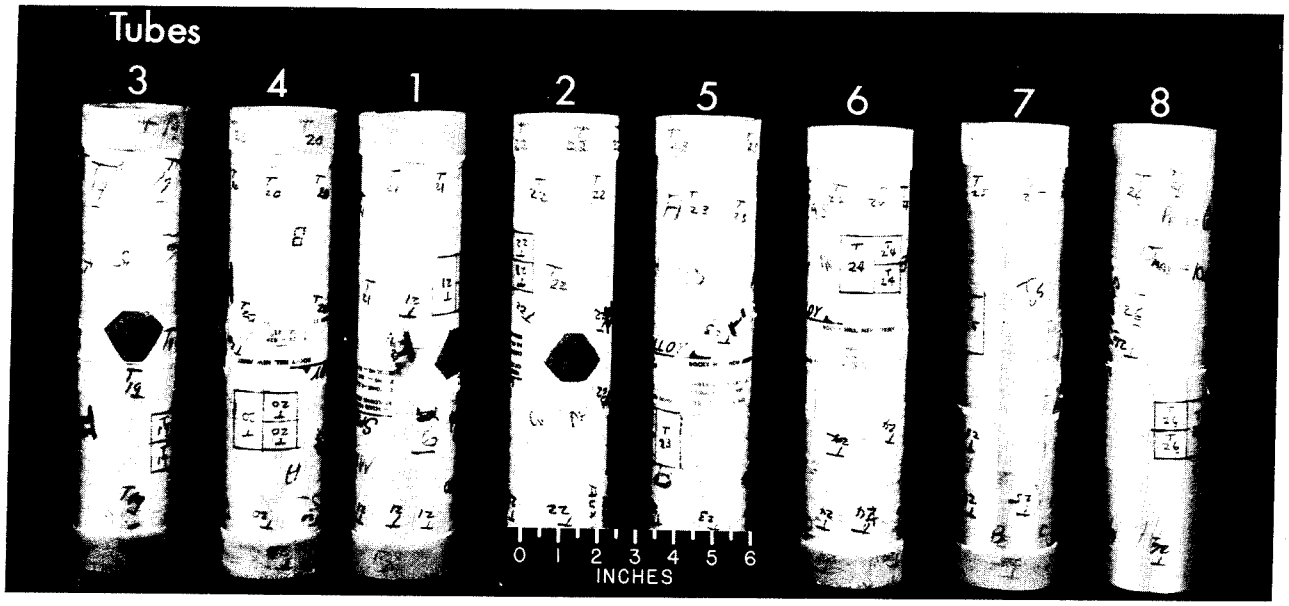

Figure 3.- Appearance of tubes after failure in compression. L-63-4886.1

From table II, it can be seen that as the helical wrap angle α is increased from 45°, the strength of the tubes decreases markedly. The strength of circumferentially wrapped tubes ($\alpha = 90^{\circ}$) is on the order of the compressive strength of the cylinder matrix. (See the matrix stress-strain curves of ref. 8.)

Unheated Cylinder Tests

To prevent end failures, the ends of the cylinders were manufactured with each end reinforced by an additional circumferential layer about $1\frac{1}{2}$ inches (3.8 cm) wide with a thickness equal to that of the cylinder wall. Certain of the specimens (cylinders 1 to 13) were subjected to small internal pressure loads prior to being tested in compression. (See ref. 8.) These cylinders were also used to determine axial stiffness under compressive loading. The load-shortening characteristics obtained are reported in reference 8. Stress-strain curves obtained from axial strain measurements were linear up to failure for cylinders with $\alpha = 25^{\circ}$. For the wrap angles of 45° or $67\frac{1}{2}^{\circ}$ stress-strain curves became nonlinear above stresses of about 6 ksi (41 MN/m^2).

All the cylinders were loaded to failure at a slow rate (3.6 kips/min (0.27 kN/s)) without cycling. Failure of the cylinders was accompanied by the appearance of two tiers of diamond-shaped buckles uniformly distributed around the cylinders. In the cylinders with a wrap angle of $67\frac{1}{2}^{\circ}$, splitting of the cylinder wall across the crests of the buckles was observed. Photographs of the typical appearance of tested cylinders with different wrap angles are presented in figure 4. The compressive strengths of the cylinders are given in table III. A few of the cylinders having wrap angles of 25° and 45° were retested and exhibited remarkable recovery (based on experience with metal cylinders) in that buckling loads ranged from 85 percent to as high as 97 percent of the originally obtained strengths.

From table III, it can be seen that as the helical wrap angle of the cylinders is increased, the compressive strength decreases although at a rate less rapid than that observed for the tubes. It can also be noted that cylinders manufactured from the resin having the largest Young's modulus (material 3) tend to have a slightly greater average strength.

Heated Cylinder Tests

The compression tests at elevated temperature were conducted by heating cylinders with a circular, quartz lamp radiator. The general features of the test setup are shown in figure 5. The radiator was insulated from the testing machine platens by two asbestos-cement plates. The plates contained circular cutouts so that the ends of the cylinder could bear on the testing machine platens. To promote uniform heating, the exterior of the cylinder was sprayed with black heat-resistant paint, and circular insulator plates were

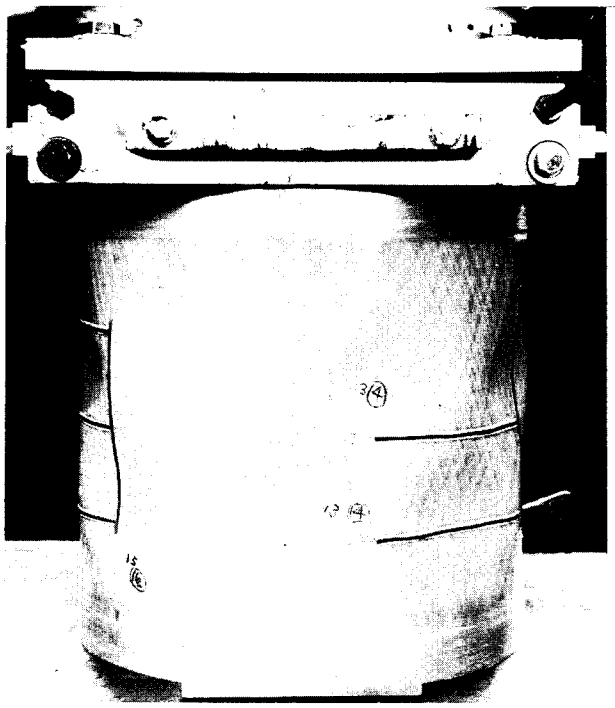

(a) $\alpha = 25^0$; cylinder 1. L-63-9884

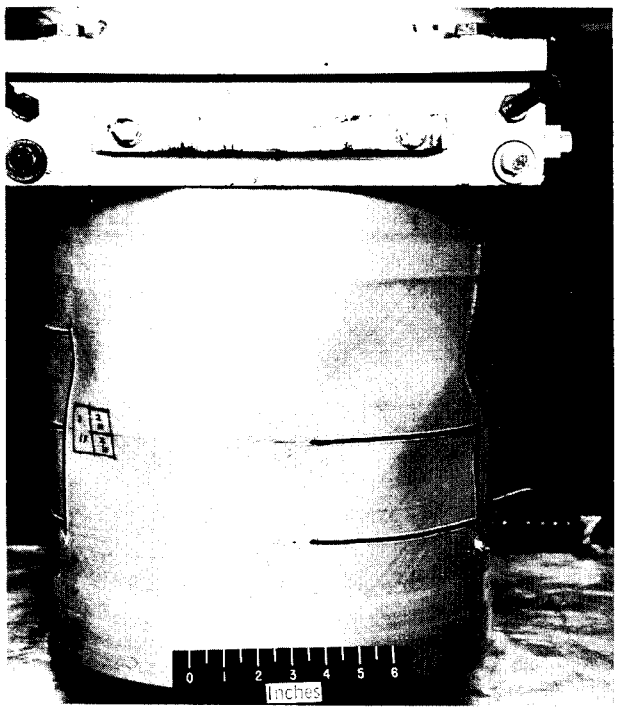

(b) $\alpha = 45^0$; cylinder 4. L-63-9885. 1

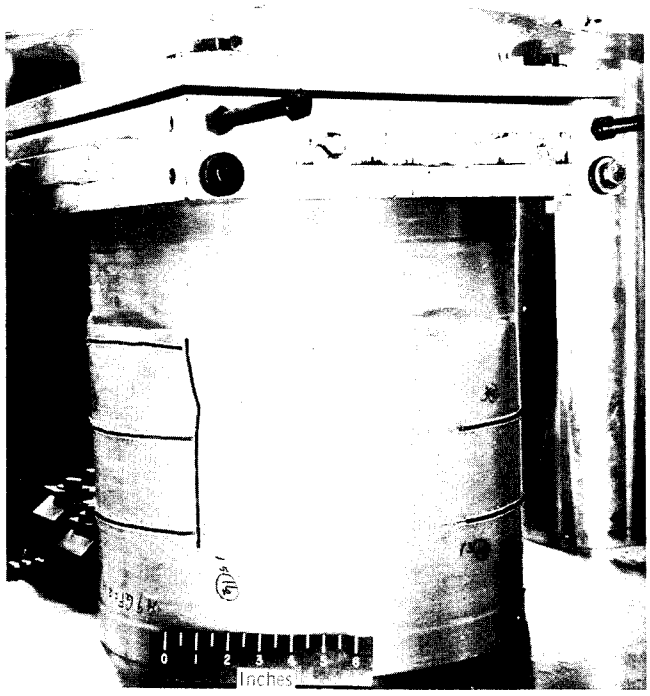

(c) $\alpha = 67\frac{1^0}{2}$; cylinder 7. L-63-9882 1

Figure 4.- Appearance of unheated cylinders after failure in compression.

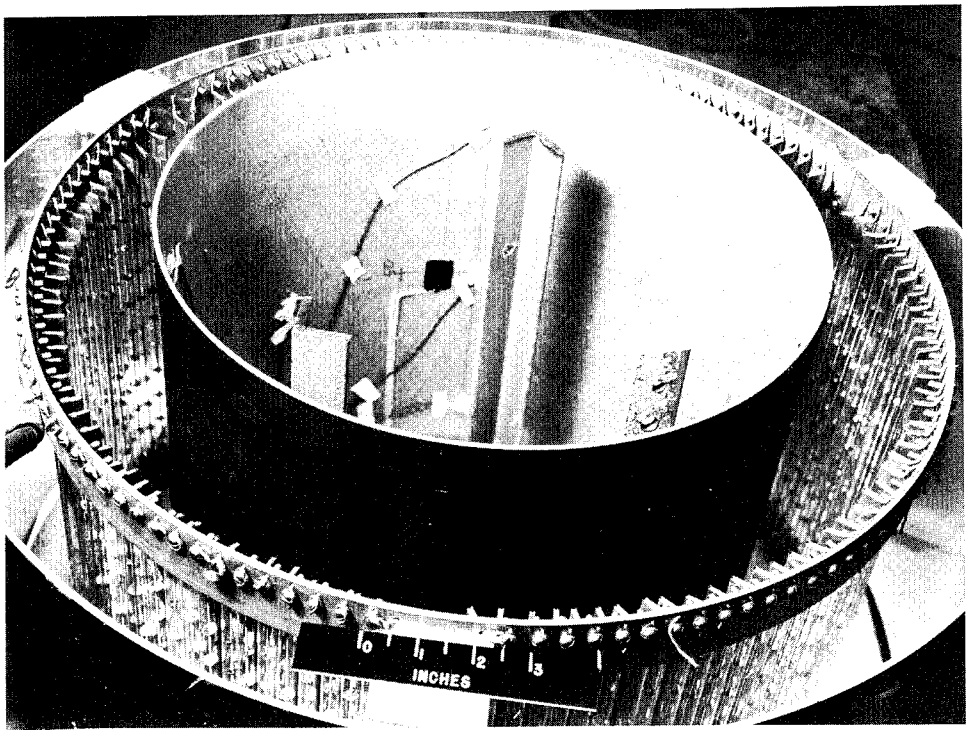

(a) Detail of radiator. L-61-8499

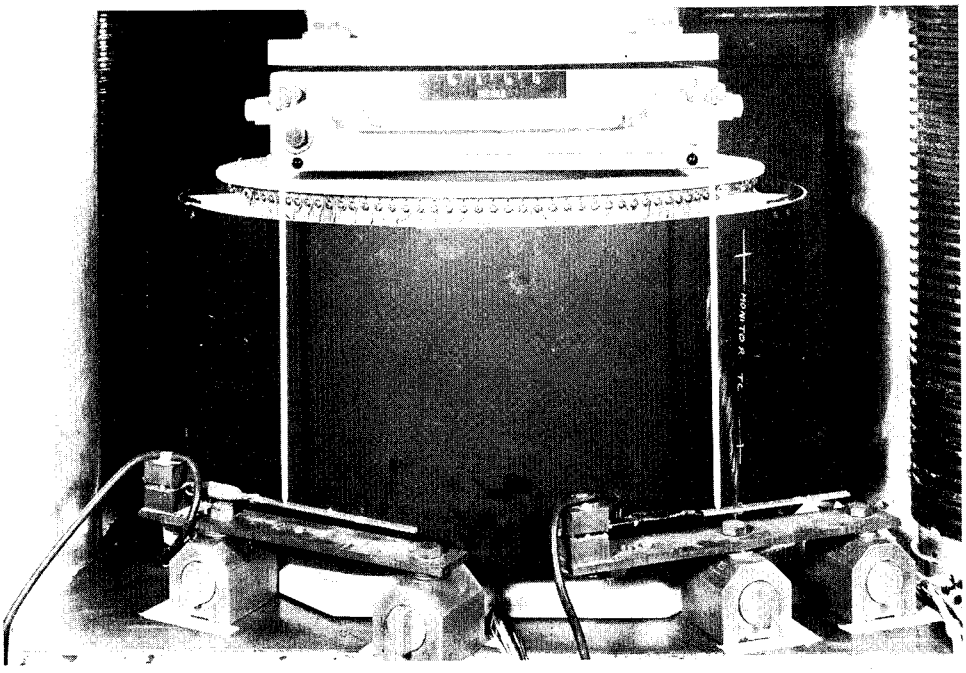

(b) Overall view. L-61-8498

Figure 5.- Setup for elevated-temperature test.

inserted in the ends of the specimens. The cylinders were instrumented with several thermocouples embedded in the wall of each cylinder to a depth of approximately half the wall thickness.

The test procedure consisted of heating the cylinder at a constant rate (15° F/min (0.14° K/s)) up to the desired test temperature; the temperature was then held constant while compressive load was slowly applied until the cylinder failed. The temperature in the cylinder wall was regulated by a lamp-voltage controller which compared a desired temperature input with that measured in a single monitor thermocouple. The test results are presented in table III. In table III, T_{av} is a temperature obtained by averaging the readings obtained from several circumferentially distributed thermocouples located at the middle of the cylinder. Representative temperature distributions existing just prior to failure are given in figure 6. In figure 6(a), the temperature at the middle of the cylinder, $T\left(\frac{l}{2},\frac{y}{2\pi r}\right)$ nondimensionalized by T_{av}, is plotted against the circumferential coordinate $\frac{y}{2\pi r}$. In figure 6(b), the temperature at any point on the cylinder, $T\left(x,\frac{y}{2\pi r}\right)$

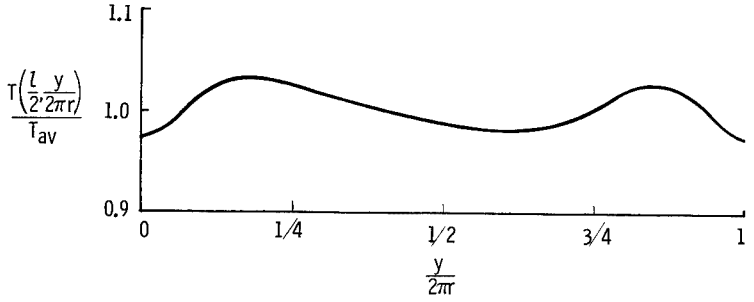

(a) Circumferential temperature distribution at middle of cylinder.

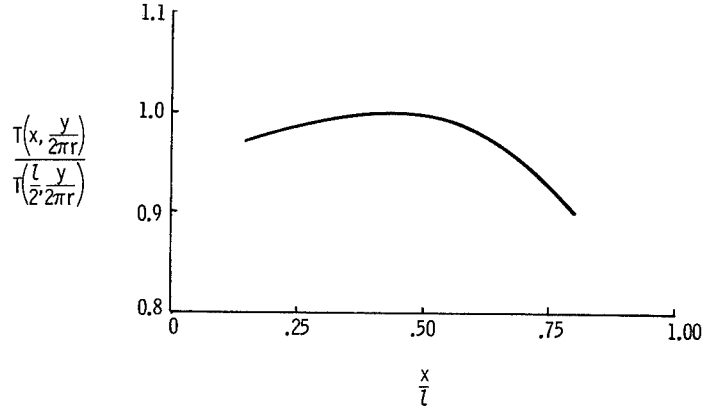

(b) Longitudinal temperature distribution.

Figure 6.- Temperature distribution in cylinders just prior to failure. (All temperatures absolute, °K or °R. See table III(b) for T_{av}.)

nondimensionalized by $T\left(\frac{l}{2},\frac{y}{2\pi r}\right)$, is plotted against the longitudinal coordinate $\frac{x}{l}$. The temperature distributions shown in figure 6 are based on absolute temperatures expressed as Kelvin or Rankine degrees. Deviations of individual test cylinder temperatures during the constant-temperature heating phase are at most ±7 percent of the value computed from curves given in figure 6.

Failure of the cylinders at the lower test temperatures was accompanied by sharp reports and by sudden reductions in load, both of which were characteristic of the tests conducted on unheated cylinders. Buckles could not be observed on the specimens because of the presence of the quartz lamp radiator. Upon unloading and cooling, the cylinders were examined and appeared to be undamaged. At the higher test temperatures, failures were less abrupt and were silent. Subsequent examination of these cylinders revealed splits in the cylinder wall and, in isolated cases, local blistering. On the basis of such observations, the mode of failure of each of the test specimens is given in table III. In the table B denotes buckling whereas M denotes a material failure in which splitting or blistering of the cylinder wall occurred. The appearance of a cylinder in which a material failure occurred is shown in figure 7.

As can be seen from table III and from data from this table plotted in figure 8, the cylinders experienced large reductions in compressive strength as the average test

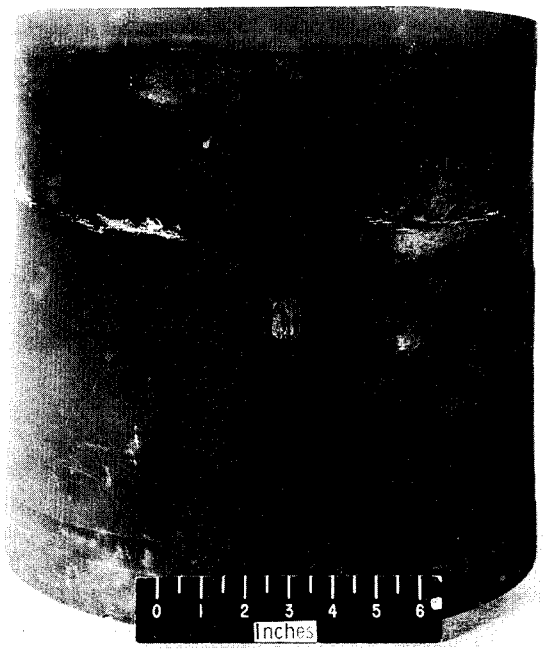

Figure 7.- Cylinder failed in compression at elevated temperature. Cylinder 42. L-61-7394

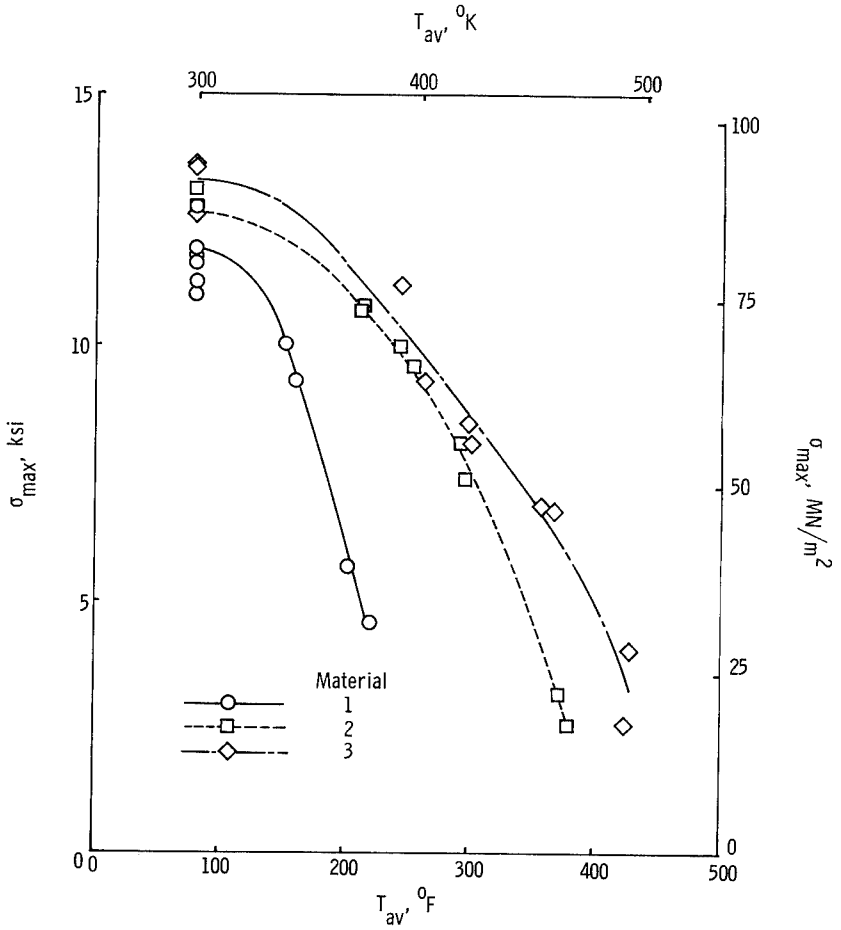

Figure 8.- Comparison of compressive strengths of heated cylinders. (Room temperature taken to be 80° F (300° K).)

temperature was increased. The test results suggest that, at some temperature, the material in the cylinder wall is so degraded by temperature that buckling failures coalesce with material failures. Above this temperature, the compressive strength of the cylinder is governed by its material strength at temperature.

COMPARISON OF TEST DATA WITH ANALYSIS

Tube Strengths

Because of their small radius-thickness ratios and moderate lengths, the tube strengths are governed by the strength of the filament-wound material. Approximate methods for predicting material strength based on anisotropic yield criteria (refs. 9, 10, and 13) are available in the literature but have not been applied generally to filament-wound structures loaded in compression. In the present report, attempts are made to

correlate the test data obtained on the tubes with strengths based on anisotropic yield criteria having the form:

$$\left(\frac{\sigma_L}{X}\right)^2 - k\left(\frac{\sigma_L \sigma_T}{XY}\right) + \left(\frac{\sigma_T}{Y}\right)^2 + \left(\frac{\tau_{LT}}{S}\right)^2 = 1 \tag{1}$$

in which σ_L and σ_T are normal stresses and τ_{LT} is the shear stress in a layer associated with directions parallel and transverse to the fibers, X and Y are allowable strengths of unidirectional layers ($\alpha = 0^o$ or 90^o) in directions parallel and transverse to the fibers, and S is an allowable shearing strength of a unidirectional layer. When the constant k is taken to be unity, equation (1) reduces to the yield criterion obtainable from reference 9. This criterion was used successfully in reference 13 to predict strengths of a variety of multilayered filament-wound plates loaded in tension. When k is taken to be zero, the yield criterion becomes that proposed in reference 10 for the design of wood structures.

The procedure employed herein for applying the yield criteria to a multilayer composite is outlined in appendix B. The procedure is based on elastic constants derived from reference 14 and is approximate in that the effects of coupling resulting from asymmetry of the layers about the middle surface of the tube (see fig. 2) are ignored and the tube matrix is assumed to behave linearly.

In making the material strength predictions, an attempt was made to consider the effect of local failures in individual layers on the overall strength of the composite. The consideration was prompted by the results of reference 13 which suggest that, under tensile loading, failures can occur in weak layers of a composite that do not precipitate immediate, overall failure of the composite. In the present calculations, upper and lower bounds on the strength of the tubes were established by considering failure to occur in one type of layer (helically or circumferentially wrapped) while requiring the other layer to remain intact. The strength of a tube in which local failures occurred should then presumably lie between these bounds. The test data and strength predictions are compared in figure 9. The dashed curve shown in figure 9 indicates the strength of the tubes when the circumferentially wrapped layers are required to remain intact and failure is assumed to occur only in the helically wrapped layers. The solid curve indicates the strengths obtained when the helically wrapped layers remain intact.

It can be seen that the strength predictions for tubes having wrap angles of 45^o are overly conservative. The agreement between the tubes having larger wrap angles is attributed to the use of the experimental data for circumferentially wrapped tubes in determining Y; the calculations are thus forced to agree with data at $\alpha = 90^o$ and cannot help but be in close agreement with data for $\alpha = 67\frac{1}{2}^o$. The structural phenomena underlying the successful application of the yield criteria in tension (ref. 13) and the unsuccessful

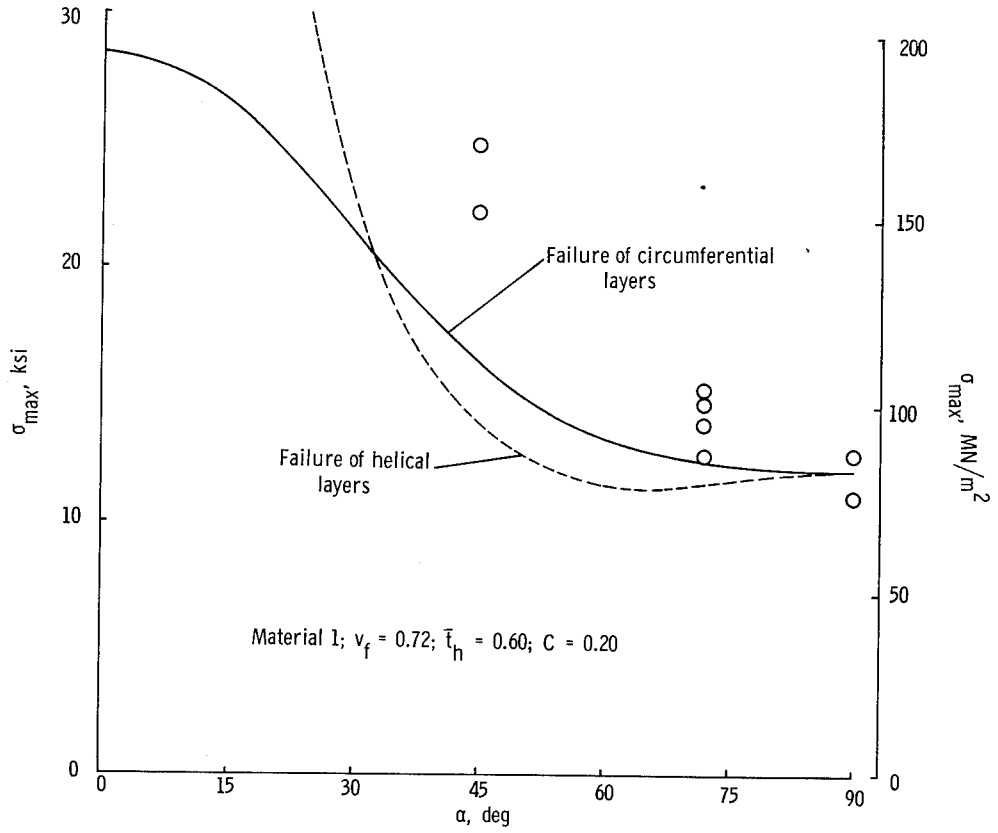

Figure 9.- Comparison of tube compressive strengths with analytical predictions based on an anisotropic yield criterion. (Ref. 9.)

attempts for compressive loading reported herein have not been satisfactorily defined by the present investigation. It appears that further investigation of methods of predicting the material strength of multilayered composites loaded in compression is required before reliable material strength predictions can be made.

Cylinder Strengths

At room temperature the cylinder strengths are governed by resistance to instability. Closed-form compressive buckling solutions available in the literature are generally restricted to cases where coupling introduced by the asymmetry of the wall configuration is ignored. In the present investigation coupling is accounted for in an approximate fashion by considering the cylinder wall to be composed of orthotropic layers. The approximation introduced for the present cylinders occurs when the two anisotropic half layers of the helically wrapped layers of the cylinder are replaced analytically by an "equivalent" orthotropic layer (see ref. 15 for a procedure to accomplish this). A stability equation is derived in appendix C for buckling of a simply supported, multilayered, orthotropic cylinder. Computed results obtained from the solution have been compared

with results obtained from a less complex stability equation which neglects coupling. The comparison suggests that the effects of coupling in the present wall configuration (see fig. 2) can be neglected. A consideration of coupling effects as the number of layers in the cylinder is varied is also given in appendix C.

The compressive strength data obtained for the unheated cylinders are compared with results computed from equation (C4) in figure 10. For $\alpha = 25^{\circ}$ the average of experimental values is roughly 80 percent of the theoretical values, whereas at $\alpha = 67\frac{1}{2}^{\circ}$, the average of experimental values is about 65 percent of theoretical values. The agreement between theory and experiment at $\alpha = 25^{\circ}$ is similar to that obtained from tests of comparable metal cylinders. In a preliminary part of the present experimental program, two aluminum-alloy cylinders having the same overall dimensions and radius-thickness ratios as the present cylinders were tested under identical conditions. The resulting compressive strengths of the metal cylinders were 85 percent of the classical buckling load for isotropic cylinders.

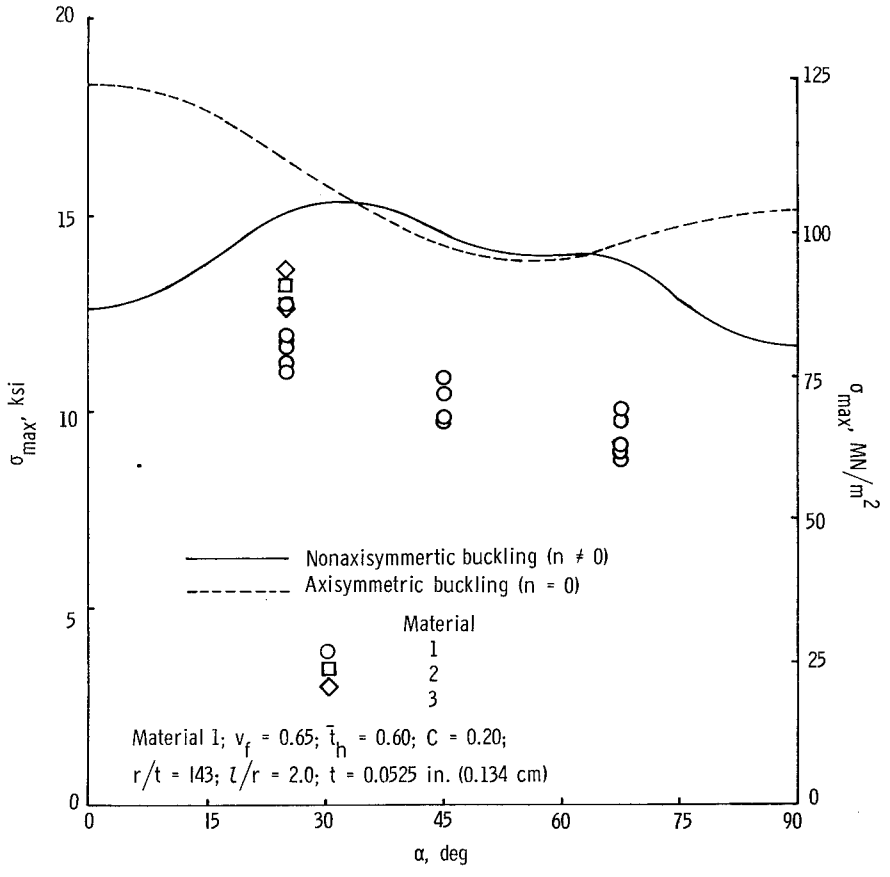

Figure 10.- Comparison of buckling calculations (eq. (C4)) with results of compression tests of unheated cylinders.

The small improvement in average compressive strengths demonstrated by cylinders constructed from material 3 over those constructed from materials 1 and 2 was not predictable by calculation. The curves shown in figure 10 were computed for material 1; the comparable curve for material 3 differed from the one shown by less than 1 percent for $\alpha = 25^{\circ}$. Hence, a change in material properties does not completely explain the improved strength. It was observed from simple block compression tests on the three epoxies (ref. 8) that material 3 has a higher proportional limit than either material 1 or 2. The greater range of linearity of materials may be a factor in the trend of the data.

Nonlinearity in the stiffness of the cylinder matrix is believed to play an important role in determining the trend of the data for α greater than 25°. Compressive stress-strain curves obtained on the cylinders exhibit considerable nonlinearity as α is increased (see ref. 8); hence, the structural stiffnesses of the cylinders are reduced from the values computed by assuming that the cylinder matrix behaves linearly. The curves shown in figure 10 were computed by assuming linear behavior of the matrix and thus less satisfactory agreement with data might be expected as α is increased.

The cracks which appeared on the cylinders having a wrap angle of $67\frac{1}{2}^{\circ}$ suggest a possibility of coincidence between material and buckling failure for these cylinders. The coincidence is unlikely, however, in view of the differences in tube strengths and cylinder strengths obtained at this wrap angle. The appearance of cracks only on the crests of buckles suggests that these are a consequence of postbuckling deformations rather than prebuckling material failures.

The test results obtained herein suggest that the buckling behavior of filament-wound cylinders is comparable to that observed in metal cylinders of similar geometry and that adequate instability predictions can be made for multilayered filament-wound cylinders provided the cylinder matrix behaves linearly. Calculations employing linear stiffnesses for cylinders having larger radius-thickness ratios and greater helical wrap angles would presumably be valid since these cylinders would necessarily buckle at lower stresses and thereby prevent the development of severe nonlinearities in the matrix. The agreement between linear theory and experiment would not be expected to be as good as that achieved in the present tests, however, in view of experience with metal cylinders of increasing radius-thickness ratios. It is clear also that nonlinearity of the cylinder matrix for certain helical wrap angles influences the buckling behavior and, if possible, should be taken into account in buckling calculations. Coalescence of buckling failures with material failures have been noted in the elevated-temperature tests and also play a part in determining the compressive strength of filament-wound cylinders at room temperatures. It appears that further research into material failure mechanisms is necessary before accurate strength predictions can be made for all filament-wound cylinder configurations.

CONCLUDING REMARKS

Data from an experimental study of the compressive strength of multilayered, filament-wound cylinders and tubes have been presented and discussed. The tests revealed the existence of two failure modes, one associated with material strength of the cylinder wall and the other with buckling of the cylinder wall. Tests conducted at elevated temperature suggest that at a certain temperature, a coalescence of buckling failures and failures resulting from thermal degradation of the cylinder material occurs. The data obtained from the tubes have been compared with strength predictions based on existing anisotropic yield criteria. The predictions were found to be overly conservative for tubes having a helical wrap angle of 45°, and this lack of agreement has not been satisfactorily explained.

Buckling predictions based on a Donnell type of theory for multilayered orthotropic cylinders have been compared with an approximate solution which neglects coupling introduced by asymmetry of the cylinder wall about the cylinder middle surface. Computed results indicate that coupling is negligible in the present cylinders and suggest that coupling effects are small for cylinders of similar geometry having as few as two layers.

Buckling predictions have been compared with the data obtained on the unheated cylinders. Agreement between analysis and experiment was comparable to that obtained with metal cylinders with differences largely attributable to nonlinearity in the stiffness of the cylinder matrix as the helical wrap angle was increased.

Langley Research Center,
National Aeronautics and Space Administration,
Langley Station, Hampton, Va., March 3, 1966.

APPENDIX A

CONVERSION OF U.S. CUSTOMARY UNITS TO SI UNITS

The International System of Units (SI) was adopted by the Eleventh General Conference on Weights and Measures, Paris, October 1960, in Resolution No. 12 (ref. 12). Conversion factors for the units used herein are given in the following table:

Physical quantity	U.S. Customary Unit	Conversion factor (*)	SI Unit
Length	inches	0.0254	meters (m)
Temperature	(^{o}F + 460)	5/9	degrees Kelvin (^{o}K)
Force	lbf	4.448	newtons (N)
Density	lbm/ft^3	16.02	kilograms per cubic meter (kg/m^3)
Stress, pressure . . .	psi=lbf/in^2	6895	newtons per square meter (N/m^2)
Unit loading	lb/in.	175.1	newtons per meter (N/m)

*Multiply value given in U.S. Customary Unit by conversion factor to obtain equivalent value in SI Unit.

Prefixes to indicate multiple of units are as follows:

Prefix	Multiple
kilo (k)	10^3
mega (M)	10^6
giga (G)	10^9
centi (c)	10^{-2}
micro (μ)	10^{-6}

APPENDIX B

STRENGTH OF A MULTILAYERED COMPOSITE

Stress Distribution

The composite is assumed to be composed of p layers symmetrically disposed about a middle surface. For the general case, each of the layers is assumed to be anisotropic so that Hooke's law in each layer can be written as

$$\begin{bmatrix} \epsilon_x \\ \epsilon_y \\ \gamma_{xy} \end{bmatrix} = \begin{bmatrix} \frac{1}{E'_x} & -\frac{\mu'_y}{E'_y} & -\frac{m_1}{E_L} \\ -\frac{\mu'_x}{E'_x} & \frac{1}{E'_y} & -\frac{m_2}{E_L} \\ -\frac{m_1}{E_L} & -\frac{m_2}{E_L} & \frac{1}{G'_{xy}} \end{bmatrix} \begin{bmatrix} \sigma_x \\ \sigma_y \\ \tau_{xy} \end{bmatrix} \tag{B1}$$

in which E_L denotes the extensional modulus of a fiber-reinforced layer in the direction parallel to the fiber (L) and where the remaining elastic constants can be expressed in terms of properties perpendicular and parallel to the fiber direction by the usual transformation equations of orthotropic elasticity. If the fibers are oriented at some angle α to the direction of loading (the x-axis), these transformation equations can be expressed as

$$\left.\begin{aligned}
\frac{1}{E'_x} &= \frac{\cos^4\alpha}{E_L} + \left(\frac{1}{G_{LT}} - \frac{2\mu_L}{E_L}\right)\sin^2\alpha\cos^2\alpha + \frac{\sin^4\alpha}{E_T} \\
\frac{1}{E'_y} &= \frac{\sin^4\alpha}{E_L} + \left(\frac{1}{G_{LT}} - \frac{2\mu_L}{E_L}\right)\sin^2\alpha\cos^2\alpha + \frac{\cos^4\alpha}{E_T} \\
\frac{1}{G'_{xy}} &= \frac{1}{G_{LT}} + \left(\frac{1+\mu_L}{E_L} + \frac{1+\mu_T}{E_T} - \frac{1}{G_{LT}}\right)\sin^2 2\alpha \\
\frac{\mu'_x}{E'_x} &= \frac{\mu'_y}{E'_y} = \frac{\mu_L}{E_L} - \frac{1}{4}\left(\frac{1+\mu_L}{E_L} + \frac{1+\mu_T}{E_T} - \frac{1}{G_{LT}}\right)\sin^2 2\alpha \\
\frac{m_1}{E_L} &= \left[\frac{\sin^2\alpha}{E_T} - \frac{\cos^2\alpha}{E_L} + \frac{1}{2}\left(\frac{1}{G_{LT}} - \frac{2\mu_L}{E_L}\right)\cos 2\alpha\right]\sin 2\alpha \\
\frac{m_2}{E_L} &= \left[\frac{\cos^2\alpha}{E_T} - \frac{\sin^2\alpha}{E_L} - \frac{1}{2}\left(\frac{1}{G_{LT}} - \frac{2\mu_L}{E_L}\right)\cos 2\alpha\right]\sin 2\alpha
\end{aligned}\right\} \tag{B2}$$

APPENDIX B

In the present paper the elastic constants $E_L, E_T, \mu_L, \mu_T, G_{LT}$ were determined from reference 14. The use of reference 14 requires evaluation of an empirical constant C, the so-called contiguity factor, which is to be determined from tests of fiber-reinforced composites. A value of 0.20 was assigned to C since elastic constants determined experimentally for certain of the test cylinders were found to be in good agreement with calculated elastic moduli based on this value. (See ref. 8.)

The stress distribution in any layer can be determined by using the methods of reference 16. If Hooke's law in each layer (eq. (B1)) is inverted so that

$$\begin{bmatrix} \sigma_x \\ \sigma_y \\ \tau_{xy} \end{bmatrix} = \begin{bmatrix} a_{11} & a_{12} & a_{13} \\ a_{21} & a_{22} & a_{23} \\ a_{31} & a_{32} & a_{33} \end{bmatrix} \begin{bmatrix} \epsilon_x \\ \epsilon_y \\ \gamma_{xy} \end{bmatrix} \tag{B3}$$

compatibility of deformation requires that the normal strains are the same in each layer and that all shearing strains are equal. If the composite is loaded in the x-direction with an average stress σ, equilibrium of the composite requires that

$$\left.\begin{aligned} \sum_{i=1}^{p} \sigma_x^{(i)} \bar{t}_i &= \sigma \\ \sum_{i=1}^{p} \sigma_y^{(i)} \bar{t}_i &= 0 \\ \sum_{i=1}^{p} \tau_{xy}^{(i)} \bar{t}_i &= 0 \end{aligned}\right\} \tag{B4}$$

where the superscript (i) denotes the ith layer and $\bar{t}_i$ is the fraction of the total thickness occupied by the ith layer.

The set of p equations implied by (B3) can be substituted into (B4) to yield

APPENDIX B

$$\begin{bmatrix} \sum_{i=1}^{p} a_{11}^{(i)}\bar{t}_i & \sum_{i=1}^{p} a_{12}^{(i)}\bar{t}_i & \sum_{i=1}^{p} a_{13}^{(i)}\bar{t}_i \\ \sum_{i=1}^{p} a_{21}^{(i)}\bar{t}_i & \sum_{i=1}^{p} a_{22}^{(i)}\bar{t}_i & \sum_{i=1}^{p} a_{23}^{(i)}\bar{t}_i \\ \sum_{i=1}^{p} a_{31}^{(i)}\bar{t}_i & \sum_{i=1}^{p} a_{32}^{(i)}\bar{t}_i & \sum_{i=1}^{p} a_{33}^{(i)}\bar{t}_i \end{bmatrix} \begin{bmatrix} \epsilon_x \\ \epsilon_y \\ \gamma_{xy} \end{bmatrix} = \begin{bmatrix} \sigma \\ 0 \\ 0 \end{bmatrix} \tag{B5}$$

Equation (B5) can then be solved for ϵ_x, ϵ_y, and γ_{xy} and the results substituted into equation (B3) to determine the stresses in each layer. These stresses are then referred to the axes of material symmetry (L and T) by using the transformations

$$\left.\begin{aligned} \sigma_L &= \sigma_x \cos^2\alpha + \sigma_y \sin^2\alpha + 2\tau_{xy} \sin\alpha \cos\alpha \\ \sigma_T &= \sigma_x \sin^2\alpha + \sigma_y \cos^2\alpha - 2\tau_{xy} \sin\alpha \cos\alpha \\ \tau_{LT} &= (\sigma_y - \sigma_x)\sin\alpha \cos\alpha + \tau_{xy}(\cos^2\alpha - \sin^2\alpha) \end{aligned}\right\} \tag{B6}$$

The stress distribution problem can be solved for the stress ratios $\frac{\sigma_x}{\sigma}$, $\frac{\sigma_y}{\sigma}$, and $\frac{\tau_{xy}}{\sigma}$.

In the application of the above procedure to the test specimens, the configuration considered was a three-layered composite composed of the circumferential layers having a relative thickness $\bar{t}_1$ equal to 0.4 and two anisotropic helically wrapped layers each having a thickness $\bar{t}_2$ or $\bar{t}_3$ equal to 0.30. The thicknesses were determined by reviewing a number of photomicrographs of the wall of the test specimens.

Application of Anisotropic Yield Criteria

The yield criteria already mentioned can be written as

$$\sigma^2 = \frac{1}{\left(\frac{\sigma_L/\sigma}{X}\right)^2 - k\left(\frac{\sigma_L \sigma_T/\sigma^2}{XY}\right) + \left(\frac{\sigma_T/\sigma}{Y}\right)^2 + \left(\frac{\tau_{LT}/\sigma}{S}\right)^2} \tag{B7}$$

where $\frac{\sigma_L}{\sigma}$, $\frac{\sigma_T}{\sigma}$, and $\frac{\tau_{LT}}{\sigma}$ are determined from equations (B6). For the tubes the following values were assigned to the allowable stresses X, Y, and S:

APPENDIX B

$X = 400\ 000$ psi (2760 MN/m^2)

$Y = 12\ 000$ psi (83 MN/m^2)

$S = 7\ 000$ psi (48 MN/m^2)

The value for X was obtained from an approximate calculation based on the results of references 1 and 17. In these references, the strength of unidirectional fiber-reinforced composites loaded in the direction of the fibers is determined by consideration of buckling of the fibers; the results obtained therein were used successfully to predict the compressive strength of boron- and hollow-glass-reinforced composites. The value for Y was taken as the approximate average of the compressive strengths obtained from the tests of the circumferentially wrapped tubes. The value assigned to S was roughly $Y/\sqrt{3}$ and was based on the observation that the circumferentially wrapped tube strengths are on the order of the compressive strength of the resin matrix and hence the shear strength is also likely to be on the order of the matrix shear strength.

Calculations using the criteria of references 9 ($k = 1$) and 10 ($k = 0$) were made, and it was observed that for α greater than 30° the calculations are relatively insensitive to the first two terms of the denominator of equation (B7). Hence, in the comparison of the yield criteria predictions with the tube data, little difference existed between the two yield criteria considered ($k = 0$ and $k = 1$) and furthermore the value assigned to X is less important than that assigned to Y and S.

In the calculations the average stresses necessary for failure in either the circumferentially or helically wrapped layers was computed. The computed values indicated that, over the range $25^\circ < \alpha < 90^\circ$, failure occurred in the helically wrapped layers before occurring in the circumferentially wrapped layers and that large differences between stresses necessary to fail either type of layer exist only in the range $0 \leqq \alpha \leqq 15^\circ$. Thus, the possibility of the composite having significant additional strength above the load at which the weakest layer fails appears unlikely in the region where $\alpha > 25^\circ$.

APPENDIX C

BUCKLING OF SIMPLY SUPPORTED MULTILAYERED ORTHOTROPIC CYLINDERS

Equilibrium equations governing the behavior of cylinders having an arbitrary number of orthotropic layers can be found in reference 11. The equations contained therein can be easily extended to obtain the equations of a small deflection buckling theory by the addition of in-plane loading terms. Donnell-type stability equations are obtained by employing the so-called "engineering theory" of reference 11. The resulting equations (based on eq. (2.11), p. 200 and eqs. (4.43) to (4.45), p. 213 of ref. 11) are

$$\left.\begin{aligned}
&C_{11}u_{,x} + C_{66}u_{,yy} + \left(C_{12} + C_{66}\right)v_{,xy} + \frac{C_{12}}{r}w_{,x} - K_{11}w_{,xxx} - \left(K_{12} + 2K_{66}\right)w_{,xyy} = 0 \\
&\left(C_{12} + C_{66}\right)u_{,xy} + C_{66}v_{,xx} + C_{22}v_{,yy} + \frac{C_{22}}{r}w_{,y} - \left(K_{12} + 2K_{66}\right)w_{,xxy} - K_{22}w_{,yyy} = 0 \\
&\frac{C_{12}}{r}u_{,x} - K_{11}u_{,xxx} - \left(K_{12} + 2K_{66}\right)u_{,xyy} + \frac{C_{22}}{r}v_{,y} - \left(K_{12} + 2K_{66}\right)v_{,xxy} \\
&- K_{22}v_{,yyy} + \frac{C_{22}}{r}w - \frac{2}{r}\left(K_{12}w_{,xx} + K_{22}w_{,yy}\right) + D_{11}w_{,xxxx} \\
&+ 2\left(D_{12} + 2D_{66}\right)w_{,xxyy} + D_{22}w_{,yyyy} + \overline{N}_x w_{,xx} + 2\overline{N}_{xy}w_{,xy} + \overline{N}_y w_{,yy} = 0
\end{aligned}\right\} \quad (C1)$$

The in-plane loading terms appear as the last three terms on the left-hand side of the third equation; the quantities $\overline{N}_x$, $\overline{N}_y$, and $\overline{N}_{xy}$ denote applied axial, circumferential, and shear forces per unit length. In equation (C1), D_{ij}, K_{ij}, and C_{ij} are stiffnesses of the cylinder wall associated with bending, coupling, and extension, respectively. These quantities are evaluated at an arbitrary reference surface by employing the integrals of equations (8.3) to (8.5), p. 34 in reference 11 and require values for the elastic constants $\overline{E}_x$, $\overline{E}_y$, $\overline{\mu}_x$, $\overline{\mu}_y$, and $\overline{G}_{xy}$ of each layer together with its thickness. In the present calculations, these elastic constants are based on reference 14 with a value of 0.20 assigned to the contiguity factor C. For a particular wrap angle, the constants were obtained by using the equations to be found in reference 15 for balanced oriented layers; the specific equations are summarized in reference 8.

Boundary conditions analogous to the conditions of simple support in classical cylinder buckling theory ($N_x = M_x = v = w = 0$ where N_x is the additional axial force per unit length during buckling and M_x is the additional axial moment per unit length during buckling) can be taken from equation (10.3), p. 38 and equations (4.34) and (4.37) p. 212 of reference 11 as

APPENDIX C

$$\left.\begin{aligned} &C_{11}u_{,x} + C_{12}v_{,y} + \frac{C_{12}}{r}w - K_{11}w_{,xx} - K_{12}w_{,yy} = 0 \\ &K_{11}u_{,x} + K_{12}v_{,y} + K_{12}\frac{w}{r} - D_{11}w_{,xx} - D_{12}w_{,yy} = 0 \\ &v = 0 \\ &w = 0 \end{aligned}\right\} \tag{C2}$$

When the cylinder is loaded with any combination of axial and circumferential loading $\left(\overline{N}_{xy} = 0\right)$, an appropriate set of displacement functions satisfying equations (C2) is

$$\left.\begin{aligned} u &= \overline{u}\cos\frac{m\pi x}{l}\cos\frac{ny}{r} \\ v &= \overline{v}\sin\frac{m\pi x}{l}\sin\frac{ny}{r} \\ w &= \overline{w}\sin\frac{m\pi x}{l}\cos\frac{ny}{r} \end{aligned}\right\} \tag{C3}$$

where m is the number of longitudinal half waves in the buckle pattern, n is the number of circumferential full waves, l is the length of the cylinder, and $\overline{u}$, $\overline{v}$, and $\overline{w}$ are amplitudes of the displacements. If equations (C3) are substituted into equations (C1) with $\overline{N}_{xy} = 0$, the existence of nontrivial buckling displacements requires that the determinant of the coefficients of $\overline{u}$, $\overline{v}$, and $\overline{w}$ vanish. This condition reduces to the stability equation

$$\left(\frac{m\pi}{l}\right)^2\overline{N}_x + \left(\frac{n}{r}\right)^2\overline{N}_y = A_{33} + \left(\frac{A_{12}A_{23} - A_{13}A_{22}}{A_{11}A_{22} - A_{12}^2}\right)A_{13} + \left(\frac{A_{12}A_{13} - A_{11}A_{23}}{A_{11}A_{22} - A_{12}^2}\right)A_{23} \tag{C4}$$

in which

$$A_{11} = C_{11}\left(\frac{m\pi}{l}\right)^2 + C_{66}\left(\frac{n}{r}\right)^2$$

$$A_{12} = \left(C_{12} + C_{66}\right)\left(\frac{m\pi}{l}\right)\left(\frac{n}{r}\right)$$

$$A_{13} = \frac{C_{12}}{r}\left(\frac{m\pi}{l}\right) + K_{11}\left(\frac{m\pi}{l}\right)^3 + \left(K_{12} + 2K_{66}\right)\left(\frac{m\pi}{l}\right)\left(\frac{n}{r}\right)^2$$

APPENDIX C

$$A_{22} = C_{66}\left(\frac{m\pi}{l}\right)^2 + C_{22}\left(\frac{n}{r}\right)^2$$

$$A_{23} = \frac{C_{22}}{r}\left(\frac{n}{r}\right) + \left(K_{12} + 2K_{66}\right)\left(\frac{m\pi}{l}\right)^2\left(\frac{n}{r}\right) + K_{22}\left(\frac{n}{r}\right)^3$$

$$A_{33} = \frac{C_{22}}{r^2} + \frac{2}{r}\left[K_{12}\left(\frac{m\pi}{l}\right)^2 + K_{22}\left(\frac{n}{r}\right)^2\right] + D_{11}\left(\frac{m\pi}{l}\right)^4 + 2\left(D_{12} + 2D_{66}\right)\left(\frac{m\pi}{l}\right)^2\left(\frac{n}{r}\right)^2 + D_{22}\left(\frac{n}{r}\right)^4$$

Equation (C4) can be used to determine buckling loads for any specified combination of axial and circumferential loading. Thus, the equation can be used to investigate buckling under axial compression, or under hydrostatic or lateral pressure, or to investigate interactions between axial compression and lateral pressure. To compute buckling loads from equation (C4), the specified loading must be minimized numerically for integral values of m and n. This minimization is best accomplished by use of a digital computer; it should be noted, however, that experience with equation (C4) indicates that certain multilayered structures may have several relative minimums so that a wide search of m and n should be made.

A useful stability equation for axisymmetric buckling of long cylinders under compressive loading can be obtained by setting $\bar{N}_y = n = 0$ in equation (C4) and requiring that $\frac{\partial \bar{N}_x}{\partial\left(\frac{m\pi}{l}\right)^2} = 0$. The resulting stability equation is

$$\bar{N}_x = \frac{2}{r}\left[\sqrt{\left(D_{11} - \frac{K_{11}^2}{C_{11}}\right)\left(C_{22} - \frac{C_{12}^2}{C_{11}}\right)} + K_{12} - \frac{C_{12}K_{11}}{C_{11}}\right] \tag{C5}$$

with the minimum m occurring when

$$\left(\frac{m\pi}{l}\right)^2 = \frac{1}{r}\sqrt{\frac{C_{22}C_{11} - C_{12}^2}{D_{11}C_{11} - K_{11}^2}}$$

If coupling is neglected (i.e., $K_{11} = K_{22} = K_{12} = K_{66} = 0$), equation (C4) can be written in the form

APPENDIX C

$$\left(\frac{m\pi}{l}\right)^2\bar{N}_x + \left(\frac{n}{r}\right)^2\bar{N}_y = \left(\frac{m\pi}{l}\right)^4\left[\frac{D_x}{1 - \tilde{\mu}_x\tilde{\mu}_y} + \left(\frac{2\tilde{\mu}_y D}{1 - \tilde{\mu}_x\tilde{\mu}_y} + 2D_{xy}\right)\left(\frac{nl}{m\pi r}\right)^2 + \frac{D_y}{1 - \tilde{\mu}_x\tilde{\mu}_y}\left(\frac{nl}{m\pi r}\right)^4\right]$$

$$+ \frac{C_x C_y}{r^2\left[C_x - \left(2\mu_y C_x - \frac{C_x C_y}{C_{xy}}\right)\left(\frac{nl}{m\pi r}\right)^2 + C_y\left(\frac{nl}{m\pi r}\right)^4\right]} \qquad \text{(C6)}$$

which reduces to the stability equation employed in reference 2 when the loading is hydrostatic or lateral pressure and to the stability equation of reference 18 when the loading is axial compression and when the transverse shearing stiffnesses of the reference are taken as infinite. For the multilayered cylinders considered herein, equation (C6) was found to be an excellent approximation. In the comparison of results computed from equation (C6) with those from equation (C4), the following approximate expressions were used to compute the structural stiffnesses

$$\left.\begin{aligned} D_x &= \frac{E_x t^3}{12} \\ D_{xy} &= \frac{G_{xy} t^3}{6} \\ D_y &= \frac{E_y t^3}{12} \\ C_x &= E_x t \\ C_{xy} &= G_{xy} t \\ C_y &= E_y t \\ \tilde{\mu}_x &= \mu_x \\ \tilde{\mu}_y &= \mu_y \end{aligned}\right\} \qquad \text{(C7)}$$

where E_x, E_y, G_{xy}, μ_x, and μ_y are given in equations (B9) of reference 8. A comparison between computed values for the specific geometry in figure 10 made from equations (C4) and (C6) is given in the following table:

APPENDIX C

α	Multilayered orthotropic theory with coupling (eq. (C4))				Orthotropic theory without coupling (eq. (C6))			
	$\bar{N}_x$				$\bar{N}_x$			
	kips/in.	MN/m	m	n	kips/in.	MN/m	m	n
0	661.0	115.7	7	11	661.2	115.8	6	10
15	722.0	126.4	6	11	714.2	125.1	7	11
30	804.3	140.8	3	9	807.3	141.4	7	11
45	746.3	130.7	16	0	763.4	133.7	16	0
60	729.7	127.8	18	0	753.2	131.9	17	0
75	672.5	117.8	9	11	664.4	116.3	9	11
90	608.8	106.6	9	11	608.5	106.6	10	11

It should be noted that equation (C4) contains coupling terms which are completely analogous to those obtained in studies of the stability of cylinders stiffened by stringers and rings. (See, for example, ref. 19.) In reference 19, rather large effects on compressive buckling loads have been reported in contrasting comparable internally and externally stiffened cylinders. By analogy, it would seem desirable, therefore, to examine the effect of rearrangement in the layers of a filament-wound cylinder to see if significant improvements in its compressive load-carrying ability would occur as a result of coupling.

A comparison of compressive strengths of multilayered cylinders having a circumferentially wrapped layer as the outer surface with those having a helically wrapped layer as the outer surface is shown in figure 11. A cylinder of the same overall geometry as the test cylinders having alternating helically and circumferentially wrapped layers is investigated; the helical wrap angle was taken to be 25°. The results indicate that requiring a circumferential layer on the outer surface gives a slightly superior design. However, in all cases the coupling effects appear to be rather small.

APPENDIX C

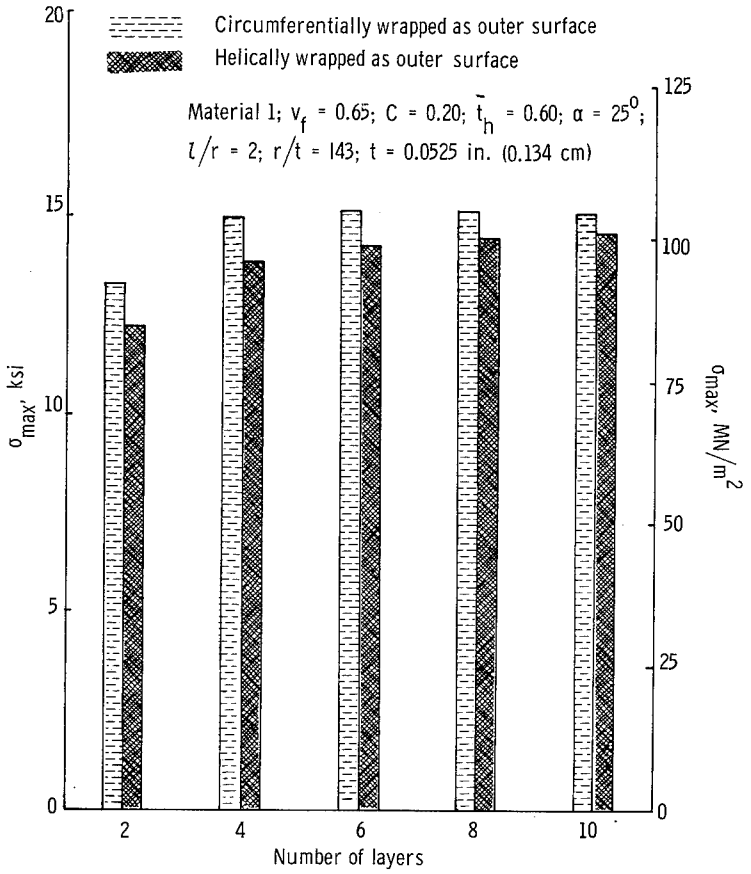

Figure 11.- Comparison of compressive strengths of multilayered cylinders having alternating helically and circumferentially wrapped layers.

REFERENCES

1. Dow, Norris F.; and Rosen, B. Walter: Evaluations of Filament-Reinforced Composites for Aerospace Structural Applications. NASA CR-207, 1965.

2. Schneider, M. H.; and Hofeditz, J. T.: Buckling of Fiberglas Cylinders Under External Pressure. 64-WA/UNT-12, Am. Soc. Mech. Engrs., 1964.

3. Ravenhall, Richard: Stiffness and Buckling in Filament-Wound Motors. J. Spacecraft, vol. 1, no. 3, May-June 1964, pp. 260-263.

4. Duffey, Chuck T.; Dunbar, George R.; and Bakken, Lawrence H.: Results of a Test Program for Filament Wound Cylinders. Materials for Space Vehicle Use. Vol. 2, Soc. Aerospace Mater. Process Engr., Nov. 1963.

5. Anon.: Design Information From Analytical and Experimental Studies on Filament Wound Structures Subjected to Combined Loading. ABL Library No. 038328, Allegany Ballistics Lab., Hercules Powder Co., Feb. 25, 1964.

6. Tasi, J.; Feldman, A.; and Stang, D. A.: The Buckling Strength of Filament-Wound Cylinders Under Axial Compression. NASA CR-266, 1965.

7. Card, Michael F.; and Peterson, James P.: On the Instability of Orthotropic Cylinders. Cylinders. Collected Papers on Instability of Shell Structures – 1962. NASA TN D-1510, 1962, pp. 297-308.

8. Card, Michael F.: Experiments to Determine Elastic Moduli for Filament-Wound Cylinders. NASA TN D-3110, 1965.

9. Hill, R.: The Mathematical Theory of Plasticity. Clarendon Press, 1956.

10. Anon.: Design of Wood Aircraft Structures. ANC-18 Bull., Second ed., Munitions Board Aircraft Comm., Dept. Defense, June 1951.

11. Ambartsumyan, S. A.: Theory of Anisotropic Shells. NASA TT F-118, 1964.

12. Mechtly, E. A.: The International System of Units – Physical Constants and Conversion Factors. NASA SP-7012, 1964.

13. Tsai, Stephen W.: Strength Characteristics of Composite Materials. NASA CR-224, 1965.

14. Tsai, Stephen W.: Structural Behavior of Composite Materials. NASA CR-71, 1964.

15. Greszczuk, L. B.: Elastic Constants and Analysis Methods for Filament Wound Shell Structures. Rept. No. SM-45849. Missile & Space Systems Div., Douglas Aircraft Co., Inc., Jan. 1965.

16. Dietz, Albert G. H., ed.: Engineering Laminates. John Wiley & Sons, Inc., 1949.

17. Schuerch, H.: Compressive Strength of Boron-Metal Composites. NASA CR-202, 1965.

18. Stein, Manuel; and Mayers, J.: Compressive Buckling of Simply Supported Curved Plates and Cylinders of Sandwich Construction. NACA TN 2601, 1952.

19. Block, David B.; Card, Michael F.; and Mikulas, Martin M., Jr.: Buckling of Eccentrically Stiffened Orthotropic Cylinders. NASA TN D-2960, 1965.

TABLE I.- SPECIMEN CONSTITUENT PROPERTIES

(a) U. S. Customary Units

Material	Matrix	Curing agent	Cure		E_m, ksi	μ_m	ρ_m, lb/cu in.	Fiber	Finish	E_f, ksi	μ_f	ρ_f, lb/cu in.
			Time, hr	Temperature, °F								
1	EPON 828	D	2	250	450	0.40	0.043	ECG 140 (12 end)	801	10 500	0.23	0.093
2	EPON 826	CL	2	300	483	.39	.043	ECG 140 (12 end)	801	10 500	.23	.093
3	Hercules Powder Co. Formulation No. 25		3	395	510	.36	.045	ECG 140 (12 end)	801	10 500	.23	.093

(b) International System of Units

Material	Matrix	Curing agent	Cure		E_m, GN/m^2	μ_m	ρ_m, Mg/m^3	Fiber	Finish	E_f, GN/m^3	μ_f	ρ_f, kg/m^3
			Time, hr	Temperature, °K								
1	EPON 828	D	2	394	3.10	0.40	1.19	ECG 140 (12 end)	801	72.40	0.23	2.57
2	EPON 826	CL	2	422	3.33	.39	1.19	ECG 140 (12 end)	801	72.40	.23	2.57
3	Hercules Powder Co. Formulation No. 25		3	475	3.52	.36	1.25	ECG 140 (12 end)	801	72.40	.23	2.57

TABLE II.- TUBE DIMENSIONS AND TEST RESULTS

(a) U.S. Customary Units

[Tube: inside diameter, 2.60 in.; length, 12 in.; material 1*]

Tube	α, deg	v_f	t, in.	P_{max}, kips	σ_{max}, ksi
1	45	0.704	0.0564	11.65	24.8
2	45	.701	.0554	10.25	22.2
3	67-1/2	.709	.0586	6.25	12.7
4	67-1/2	.728	.0564	6.86	14.6
5	67-1/2	.728	.0556	7.05	15.2
6	67-1/2	.721	.0558	6.46	13.9
7	90	.721	.0671	7.14	12.7
8	90	.670	.0709	6.55	11.0

(b) International System of Units

[Tube: inside diameter, 6.60 cm; length, 30.5 cm; material 1*]

Tube	α, deg	v_f	t, cm	P_{max}, kN	σ_{max}, MN/m^2
1	45	0.704	0.1433	51.8	171.0
2	45	.701	.1407	45.6	153.0
3	67-1/2	.709	.1488	27.8	87.6
4	67-1/2	.728	.1433	30.5	101.0
5	67-1/2	.728	.1412	31.4	105.0
6	67-1/2	.721	.1417	28.7	95.8
7	90	.721	.1704	31.8	87.6
8	90	.670	.1801	29.1	75.9

*See table I.

TABLE III.- CYLINDER DIMENSIONS AND TEST RESULTS

[Cylinder: inside diameter, 15.0 in.; length, 15.0 in.]

(a) U.S. Customary Units

Cylinder	Material (a)	α, deg	t, in.	v_f	P_{max}, kips	σ_{max}, ksi	T_{av}, ^oF	Failure mode (b)
1	1	25	0.0551	0.638	33.2	12.7	Room	B
2	1	25	.0549	.650	30.8	11.9	↓	B
3	1	25	.0551	.633	33.2	12.7	↓	B
4	1	45	.0546	.632	26.9	10.4	↓	B
5	1	45	.0553	.625	27.1	10.8	↓	B
6	1	45	.0477	.655	23.4	10.4	↓	B
7	1	67-1/2	.0557	.663	25.6	9.7	↓	B and M
8	1	67-1/2	.0540	.660	23.3	9.1	↓	B and M
9	1	67-1/2	.0552	.694	26.2	10.0	↓	B and M
10	2	25	.0505	.665	31.4	13.2	↓	B
11	3	25	.0548	.639	33.6	12.6	↓	B
12	1	25	.0517	.650	28.4	11.6	↓	B
13	1	25	.0537	.636	30.3	11.9	↓	B
14	1	25	.0538	.643	28.0	11.0	↓	B
15	1	25	.0541	.653	28.6	11.2	↓	B
16	1	25	.0578	.603	25.5	9.3	161	B
17	1	25	.0506	.641	23.9	10.0	152	B
18	1	25	.0577	.605	12.5	4.6	222	M
19	1	25	.0558	.608	15.0	5.7	203	M
20	1	45	.0487	.668	22.5	9.8	Room	B
21	1	45	.0491	.668	22.5	9.7	Room	B
22	1	67-1/2	.0525	.678	22.1	8.9	Room	B and M
23	1	67-1/2	.0516	.663	21.3	8.7	Room	B and M
24	2	25	.0475	.692	28.5	12.7	Room	B
25	2	25	.0501	.690	28.0	11.8	Room	B
26	2	25	.0497	.675	25.2	10.7	213	B
27	2	25	.0501	.677	25.6	10.8	215	B
28	2	25	.0497	.668	22.5	9.6	250	B
29	2	25	.0500	.668	23.6	10.0	244	B
30	2	25	.0495	.701	17.3	7.4	297	B and M
31	2	25	.0502	.665	19.2	8.1	292	B and M
32	2	25	.0496	.695	6.0	2.6	379	M
33	2	25	.0510	.698	7.6	3.2	372	M
34	3	25	.0545	.650	34.8	13.5	Room	B
35	3	25	.0539	.652	34.6	13.6	Room	B
36	3	25	.0553	.637	24.4	9.3	262	B
37	3	25	.0599	.595	31.7	11.2	245	B
38	3	25	.0552	.637	21.1	8.1	301	B and M
39	3	25	.0577	.612	23.2	8.5	299	B
40	3	25	.0564	.601	18.2	6.8	368	B and M
41	3	25	.0567	.599	18.4	6.9	358	B and M
42	3	25	.0652	.591	12.7	4.1	428	M
43	3	25	.0608	.593	7.4	2.6	425	M

[a] See table I.

[b] B denotes buckling; M denotes material failure.

TABLE III.- CYLINDER DIMENSIONS AND TEST RESULTS – Concluded

[Cylinder: inside diameter, 38.1 cm; length, 38.1 cm]

(b) International System of Units

Cylinder	Material (a)	α, deg	t, cm	v_f	P_{max}, kN	σ_{max}, MN/m^2	T_{av}, ^oK	Failure mode (b)
1	1	25	0.140	0.638	148	87.57	Room	B
2	1	25	.139	.650	137	82.05		B
3	1	25	.140	.633	148	87.57		B
4	1	45	.139	.632	120	71.71		B
5	1	45	.141	.625	121	74.47		B
6	1	45	.121	.655	104	71.71		B
7	1	67-1/2	.142	.663	114	66.88		B and M
8	1	67-1/2	.137	.660	104	62.74		B and M
9	1	67-1/2	.140	.694	117	68.95		B and M
10	2	25	.128	.665	140	91.01		B
11	3	25	.139	.639	149	86.88		B
12	1	25	.131	.650	126	80.05		B
13	1	25	.136	.636	135	82.19		B
14	1	25	.137	.643	125	75.84		B
15	1	25	.137	.653	127	77.01		B
16	1	25	.147	.603	113	64.26	345	B
17	1	25	.129	.641	106	68.81	340	B
18	1	25	.147	.605	55.6	31.58	379	M
19	1	25	.142	.608	66.7	39.16	369	M
20	1	45	.124	.668	100	67.36	Room	B
21	1	45	.125	.668	100	66.81		B
22	1	67-1/2	.133	.678	98.3	61.36		B and M
23	1	67-1/2	.131	.663	94.7	60.19		B and M
24	2	25	.121	.692	127	87.43		B
25	2		.127	.690	125	81.43		B
26	2		.126	.675	112	73.91	374	B
27	2		.127	.677	114	74.46	375	B
28	2		.126	.668	100	65.98	394	B
29	2		.127	.668	105	68.74	391	B
30	2		.126	.701	76.9	50.95	421	B and M
31	2		.128	.665	85.4	55.71	418	B and M
32	2		.126	.695	26.7	17.65	466	M
33	2		.129	.698	33.8	21.72	462	M
34	3		.138	.650	155	93.01	Room	B
35	3		.137	.652	154	93.56	Room	B
36	3		.140	.637	109	64.33	401	B
37	3		.152	.595	141	77.15	392	B
38	3		.140	.637	93.9	55.71	423	B and M
39	3		.147	.612	103	58.61	422	B
40	3		.143	.601	80.9	47.02	460	B and M
41	3		.144	.599	81.8	47.30	455	B and M
42	3		.166	.591	56.5	28.41	494	M
43	3		.154	.593	32.9	17.72	492	M

[a] See table I.

[b] B denotes buckling; M denotes material failure.